Journal of Applied Physics

Systematic characterization of a 1550 nm microelectromechanical (MEMS)-tunable vertical-cavity surface-emitting laser (VCSEL) with 7.92 THz tuning range for terahertz photomixing systems

Cite as: J. Appl. Phys. **123**, 023106 (2018); https://doi.org/10.1063/1.5003147
Submitted: 03 September 2017 . Accepted: 23 December 2017 . Published Online: 11 January 2018

M. T. Haidar, S. Preu, J. Cesar, S. Paul, A. S. Hajo, C. Neumeyr, H. Maune, and F. Küppers

AIP Publishing

Systematic characterization of a 1550 nm microelectromechanical (MEMS)-tunable vertical-cavity surface-emitting laser (VCSEL) with 7.92 THz tuning range for terahertz photomixing systems

M. T. Haidar,[1,a)] S. Preu,[2,b)] J. Cesar,[1] S. Paul,[1] A. S. Hajo,[1] C. Neumeyr,[3] H. Maune,[1] and F. Küppers[1]

[1]*Institute for Microwave Engineering and Photonics, Technische Universität Darmstadt, Merckstrasse 25, 64283 Darmstadt, Germany*
[2]*Department of Electrical Engineering and Information Technology, Technische Universität Darmstadt, Terahertz Systems Technology, Merckstrasse 25, 64283 Darmstadt, Germany*
[3]*VERTILAS GmbH, Daimlerstrasse 11d, 85748 Garching, Germany*

(Received 3 September 2017; accepted 23 December 2017; published online 11 January 2018)

Continuous-wave (CW) terahertz (THz) photomixing requires compact, widely tunable, mode-hop-free driving lasers. We present a single-mode microelectromechanical system (MEMS)-tunable vertical-cavity surface-emitting laser (VCSEL) featuring an electrothermal tuning range of 64 nm (7.92 THz) that exceeds the tuning range of commercially available distributed-feedback laser (DFB) diodes (∼4.8 nm) by a factor of about 13. We first review the underlying theory and perform a systematic characterization of the MEMS-VCSEL, with particular focus on the parameters relevant for THz photomixing. These parameters include mode-hop-free CW tuning with a side-mode-suppression-ratio >50 dB, a linewidth as narrow as 46.1 MHz, and wavelength and polarization stability. We conclude with a demonstration of a CW THz photomixing setup by subjecting the MEMS-VCSEL to optical beating with a DFB diode driving commercial photomixers. The achievable THz bandwidth is limited only by the employed photomixers. Once improved photomixers become available, electrothermally actuated MEMS-VCSELs should allow for a tuning range covering almost the whole THz domain with a single system. *Published by AIP Publishing.* https://doi.org/10.1063/1.5003147

I. INTRODUCTION

Since the first demonstration of a vertical-cavity surface-emitting laser (VCSEL) by Iga in 1977,[1] many practical applications have benefited from its inherent characteristics: low power consumption, on-wafer testing, excellent coupling efficiency to fibers, dynamic single-mode operation, and compactness, to name but a few. Fixed-cavity-length GaAs-based VCSELs around 850 nm have become the workhorse for short optical interconnects and local area networks (LANs).[2] While fixed-cavity-length VCSELs offer excellent performance for narrow-bandwidth applications, for applications requiring a large tuning range of several 10 nm it is necessary to employ a microelectromechanical system (MEMS)-tunable VCSEL consisting of a fixed mirror and a MEMS-actuated mirror. Electrothermally tunable MEMS-VCSELs have shown their effectiveness in optical communication systems,[3,4] sensing and spectroscopy,[5] and optical coherence tomography (OCT).[6] In addition to those established fields, we have already investigated the application of MEMS-VCSELs in terahertz (THz) photomixing systems.[7]

Terahertz applications between 100 GHz and 10 THz include noninvasive medical imaging, future high-frequency communications, spectroscopy, homeland security, and earth- and space science applications, among many other fields.[8,9] For applications where a large frequency coverage of up to several THz or a high spectral resolution is required, THz generation by heterodyne photomixing of two continuous-wave (CW) lasers is commonly used.[10] Two lasers at frequencies ν_1 and $\nu_2 = \nu_1 + \nu_{THz}$ drive an ultra-fast photodiode (PD) or a photoconductor that generates an alternating current (ac) oscillating with the difference frequency of ν_{THz}.[11] A suitably designed antenna converts the ac current into free-space THz emission. For detection, a photoconductor mixes the received THz signal with the optical envelope of the beat signal that was previously used for the THz generation, leading to a down-conversion of the THz field to a dc photocurrent as a read-out signal. Such photomixing systems are typically limited in bandwidth to ≈3 THz. Commercial narrow-linewidth telecommunications-wavelength lasers, such as distributed-feedback laser (DFB) diodes, however, are tunable by not more than 0.6 THz. By appropriate selection of the individual wavelengths, it has been shown that three such diodes are indeed sufficient to cover a frequency span of up to 3 THz.[12] However, switching lasers has a deleterious effect on THz measurements. Most laser systems that include external cavity lasers with a tuning range of several THz are relatively bulky and expensive although recent developments in compact semiconductor lasers may solve this problem for future THz systems. Such lasers include, for example, sampled-grating distributed-Bragg-reflector (SG-DBR) lasers,[13] Y-branch lasers,[14] and MEMS-VCSELs.[4] The particular advantages of MEMS-VCSELs are their extremely fast tunability and their almost-circular mode profile, which is eminently suited for fiber coupling.

In a previous publication, we reported on a non-optimized THz system using a MEMS-VCSEL.[7] To demonstrate the huge

a)Electronic mail: haidar@imp.tu-darmstadt.de
b)Electronic mail: preu@imp.tu-darmstadt.de

tuning range of the MEMS-VCSEL, which is much larger than the bandwidth of a photomixer, the MEMS-VCSEL was swept from 1.61 THz below to 1.62 THz above the frequency of a DFB diode, yielding a total scanned frequency span of 3.23 THz. In the present work, we demonstrate homodyne detection over a total span of 4.74 THz by heterodyning of a polarization-stable, tunable MEMS-VCSEL and a DFB diode. The paper is structured as follows. In the Secs. II A–II D, we review the underlying theory and systematically characterize two MEMS-VCSELs denoted as VCSEL-A and VCSEL-B, considering all aspects relevant for THz photomixing. These include tunability, side-mode suppression ratio (SMSR), output power, linewidth, wavelength stability, and polarization stability. In Sec. II E, we describe the THz setup and the results obtained using a commercial DFB diode heterodyned with VCSEL-A, which is optimized for THz applications.

II. KEY FEATURES OF MEMS-VCSELS

A. The MEMS-VCSEL structure

A cross-sectional schematic diagram of a MEMS-VCSEL is shown in Fig. 1; a detailed explanation can be found in Ref. 4. A tunable MEMS-VCSEL is commonly composed of a movable distributed-Bragg-reflector (DBR) top mirror with evaporation-deposited actuation contacts, an air gap, a semiconductor cavity (SC), and an integrated DBR bottom mirror. To reduce reflectivity at the SC–air interface, an antireflection (AR) coating is used. The SC, which contains AlInGaAs-based multi-quantum wells (MQWs) as gain medium, a buried tunnel junction (BTJ), and two InP heat- and current-spreading layers, together with the bottom mirror is termed the half-VCSEL. The BTJ, with a diameter of $D_{\mathrm{BTJ}} = 14\,\mu$m, serves as a current aperture. A description of the active region and BTJ structure is given in Ref. 15. The half-VCSEL is mounted on an electroplated gold substrate. The semiconductor (InP) around the mesa is replaced by a low-dielectric-constant passivation layer of benzocyclobutene (BCB) to eliminate parasitic capacitances. The movable top mirror consists of 11.5 SiN_x/SiO_y dielectric layer pairs. Each layer has an optical thickness of $\lambda_0/4$, where $\lambda_0 = 1550$ nm is the center wavelength. Intentional stress gradients are incorporated during the growth of these layers, causing the mirror to bend upwards with a well-defined radius of curvature (RoC), resulting in a plane-concave laser cavity. A heating current applied through the Cr/Au electrodes evaporated onto the top of the mirror enables electrothermal actuation by thermal expansion of the suspended membrane. A 50 μm-diameter circular hole in the metal electrode (the dish diameter is 110 μm), as shown in the scanning electron microscope (SEM) image in Fig. 2, serves as the exit aperture of the laser cavity. It is connected to four flexible beams of length and width 150 and 60 μm, respectively, which support the mirror suspension. Throughout this paper, the suspended mirror will be termed the membrane DBR, or simply the membrane. The bottom DBR and the membrane form a plane-concave Fabry–Pérot resonator with a total optical cavity length L, which is the sum of the encapsulated air gap L_{air}, the SC length L_{SC}, and the penetration depths $L_{\mathrm{DBR,t}}$ and $L_{\mathrm{DBR,b}}$ of the optical field into the top and bottom DBRs, respectively, as illustrated in Fig. 1.

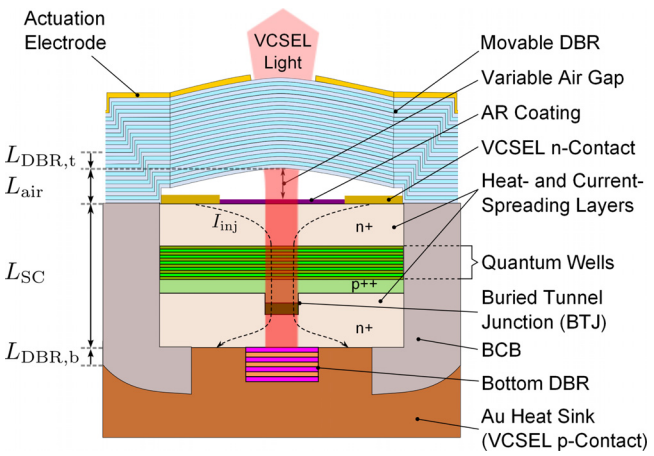

FIG. 1. Cross-sectional schematic of a MEMS-VCSEL.

B. Electrothermal tuning characteristics

A laser diode controller (LDC) injects the current I_{inj} for electrical pumping of the on-wafer MEMS-VCSEL. Another LDC provides the heating/tuning current I_{MEMS} through the electrode of the membrane (the membrane actuation current). The subsequent Joule heating P_{heat} expands the membrane, causing an increase in the air gap, i.e., the cavity length. The corresponding change in the emission wavelength is given by

$$\Delta\lambda \propto \Delta L_{\mathrm{air}} \propto P_{\mathrm{heat}} = I_{\mathrm{MEMS}}^2 R_{\mathrm{MEMS}}, \tag{1}$$

where $R_{\mathrm{MEMS}} \approx 25\,\Omega$ is the electrical resistance of the heating electrode of the membrane.

Figure 3 shows the electrothermal actuation of a MEMS-VCSEL (VCSEL-A) with a mode-hop-free tuning from 1525 nm ($I_{\mathrm{MEMS}} = 0$ mA) to 1589 nm ($I_{\mathrm{MEMS}} = 37.6$ mA) with $I_{\mathrm{inj}} = 20$ mA and a substrate temperature of $T_s = 22\,^{\circ}$C. This yields a tuning range of 64 nm (7.92 THz) covering the spectral bandwidth (1530–1565 nm) of the erbium-doped fiber amplifier (EDFA) that is employed to boost the VCSEL power during the

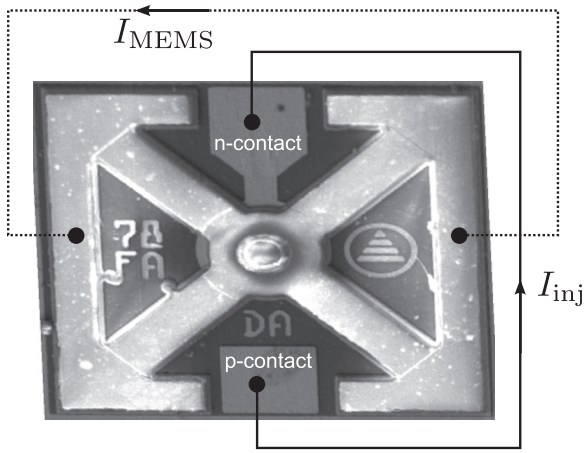

FIG. 2. SEM image showing the top view of an on-wafer MEMS-VCSEL. The two wire connections for the injection and actuation currents are shown schematically.

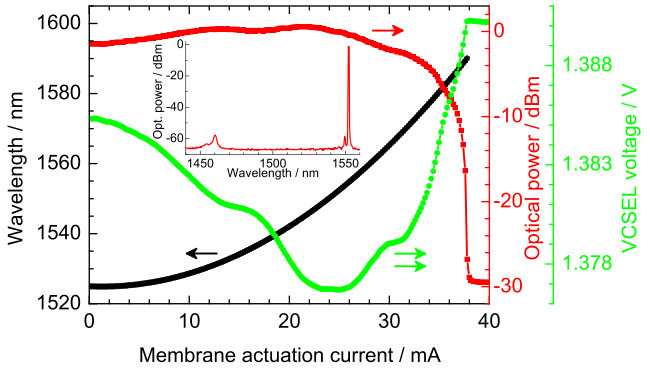

FIG. 3. Mode-hop-free electrothermal actuation of VCSEL-A: single-mode CW power (red), VCSEL voltage (green), and peak emission wavelength (black) for $I_{inj} = 20$ mA.

THz photomixing experiment. The corresponding CW power and voltage profile are also shown in Fig. 3. The inset in the figure shows an emission spectrum of VCSEL-A at a fixed membrane current. The spectral distance to the next-higher-order longitudinal mode, i.e., the free spectral range (FSR), is 92 nm, which is the ultimate limit for mode-hop-free tuning. The highest SMSR of 58 dB is obtained at this wavelength. However, a minimum SMSR of >50 dB is maintained over the entire tuning range, which is 11 dB higher than the value presented in Ref. 16. The minimum VCSEL voltage obtained with $I_{MEMS} \approx 24$ mA corresponds to the lowest threshold gain. The voltage drop of the laser from Fig. 3 clearly correlates with the laser threshold current as shown in Fig. 4. In Fig. 4, the differential quantum efficiency η_d is also plotted as a function of the membrane actuation current. The differential quantum efficiency is a function of the slope of the light–current (*L–I*) curve above the threshold as follows:

$$\eta_d = \frac{\Delta P}{\Delta I_{inj}} \left[\frac{e\lambda}{hc}\right], \tag{2}$$

where P is the emitted optical power captured by the large-area PD, e is the elementary electric charge, h is the Planck's constant, and c is the speed of light. A value of $\eta_d > 9\%$ is obtained over the tuning range of interest (1530–1565 nm), with a maximum of $\eta_d = 18\%$ with $I_{MEMS} = 12$ mA ($\lambda = 1530.5$ nm), as shown in Fig. 4. From Eq. (2), the electrical-to-optical conversion inside the cavity (higher slope efficiency) is highest at this point. The outcoupled power, however, does not achieve its highest value here. At longer wavelengths, the membrane becomes less reflective. This decreases the Q-factor of the cavity, but it also increases the outcoupled power since the transmission $T = 1 - R_t$, with R_t being the reflectivity of the membrane. However, thermal rollover with increased injection current[16] appears much earlier when compared with the point of minimum threshold gain. Despite obtaining more power with $I_{inj} > 20$ mA, we limit the injection current to $I_{inj} = 20$ mA to avoid thermal rollover during THz photomixing.

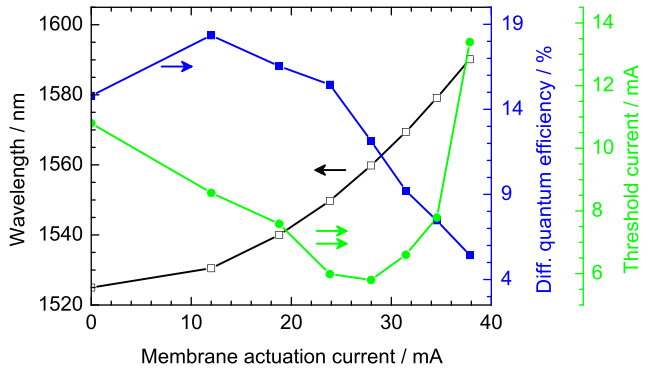

FIG. 4. Laser threshold current (green), differential quantum efficiency (blue), and emission wavelength (black).

The frequency response of the membrane to current actuation is investigated by a sinusoidal modulation of the membrane current and monitoring of the laser emission. The MEMS-VCSEL (VCSEL-A) is biased with $I_{inj} = 20$ mA and $I_{MEMS} = 25$ mA at $T_s = 22\,^\circ$ C. With a peak-to-peak modulation current of 20 mA, the membrane oscillates between 15 and 35 mA, giving a wavelength variation between 1525 and 1589 nm at low modulation frequencies, as illustrated in Fig. 5. With an initial wavelength tuning range of $\Delta\lambda_{max} = 64$ nm, the thermal inertia of the membrane follows a low-pass filter behavior of the first order:

$$\Delta\lambda(f) = \frac{\Delta\lambda_{max}}{\sqrt{1 + 3\left(f/f_{mod,3dB}\right)^2}} \tag{3}$$

with a 3 dB frequency of $f_{mod,3\text{-}dB} = \sqrt{3}/(2\pi\tau)$, where τ is the thermal time constant of the membrane. The corresponding fit to the experimental data gives $f_{mod,3dB} = 258.65 \pm 7.09$ Hz featuring a time constant of $\tau = 1.06$ ms, as illustrated in Fig. 6. The value of $f_{mod,3dB}$ indicates that the entire tuning range of the MEMS-VCSELs can be tuned within just a few milliseconds.

C. Linewidth and frequency stability

Terahertz signals generated by the CW photomixers feature a linewidth that corresponds to the combined linewidth of the two lasers. The influence of the photomixing process is typically negligible. For many applications, in particular

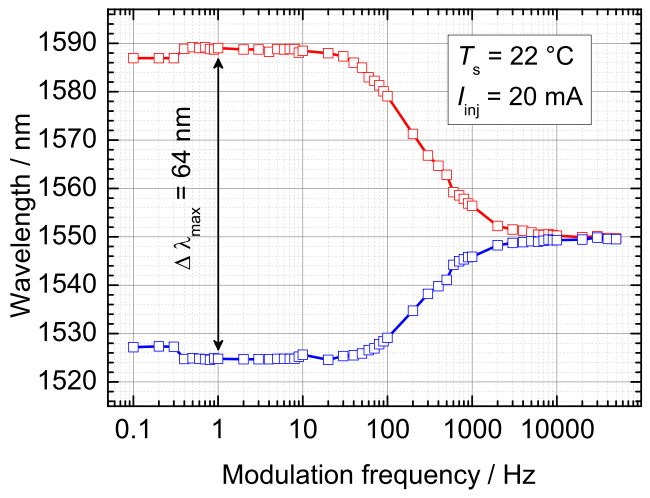

FIG. 5. Electrothermal frequency response of VCSEL-A for an initial wavelength tuning of $\Delta\lambda = 64$ nm.

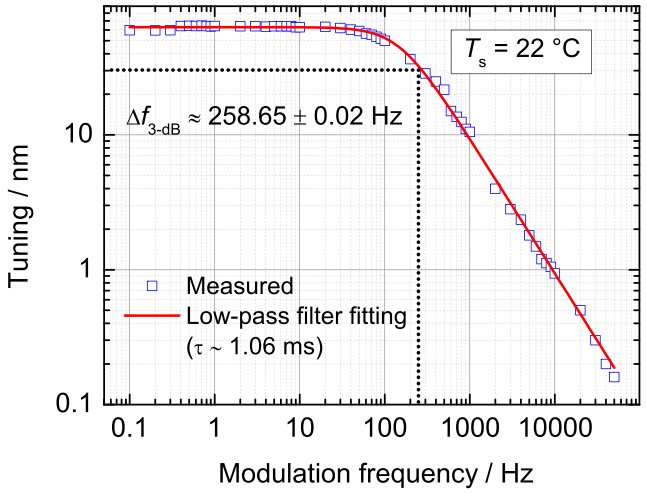

FIG. 6. First-order low-pass filter behavior of the modulation performance.

for THz spectroscopy, a narrow linewidth and good frequency stability of the lasers are highly important. For example, most polar gases feature linewidths in the few-GHz range under normal conditions.[17] At lower pressures in the millibar range, the linewidths fall to a few tens of kHz,[17] requiring additional linewidth-stabilization techniques. Fixed-frequency VCSELs show a typical linewidth in the range of a few MHz,[18,19] attributable to the high quality factor of the laser cavity. Such linewidths would be sufficient for THz spectroscopy experiments under normal pressure. The suspended membrane of the MEMS-VCSEL, however, is prone to additional influence of noise that leads to a larger linewidth. In the following, we will determine the influence of mechanical and thermal noise on the linewidth of the MEMS-VCSELs and compare our findings with experimental results.

The motion of the membrane can be described as a mechanical resonator according to the following equation:[20,21]

$$m\ddot{x} + R_m\dot{x} + k_m x = F(t), \tag{4}$$

where x is the displacement of the membrane from its equilibrium position, m, R_m, and k_m are the mass, damping constant, and spring constant of the membrane, and $F(t)$ is the force acting on the membrane. Since the membrane is suspended in air, we expect little damping and therefore neglect the second term in Eq. (4). The fundamental mechanical resonance frequency of the membrane is thus

$$\nu_{res,1} \approx \frac{1}{2\pi}\sqrt{\frac{k_m}{m}}. \tag{5}$$

The mass of the membrane calculated from its dimensions is $m \approx 0.55\,\mu$g. According to Refs. 5 and 22, only half of each suspension beam experiences the vibration of the membrane, leading to an effective mass $m_{eff} = 0.34\,\mu$g. The spring constant can be determined by a measurement of the mechanical resonance spectrum of the membrane. The bare membrane is characterized by capturing its velocity signal by a laser Doppler vibrometer (LDV, Polytec: OFV-2502 controller, OFV-534 sensor head with a sensitivity of 25 mm s^{-1} V^{-1}) at atmospheric pressure without any laser injection current. A bias voltage $U(t) = U_{dc} + U_{mod}\sin(\omega_{mod}t)$ ($U_{dc} = 20$ V, peak-to-peak $U_{mod} = 1.5$ V) is applied between the n-contact and the membrane electrodes of the MEMS-VCSEL, forming a capacitor. This exerts an electrostatic force on the membrane. Figure 7 shows the velocity signal of the membrane (VCSEL-B) as a function of the modulation frequency. Two mechanical resonance frequencies for VCSEL-B are found experimentally at $\nu_{res,1} = 283$ kHz and $\nu_{res,2} = 1215$ kHz, where $\nu_{res,1}$ is the fundamental resonance frequency. These resonances can cause power and wavelength fluctuations as demonstrated in Ref. 20 using a fixed-frequency laser feeding to a MEMS-tunable Fabry–Pérot etalon. Mechanical noise or external influence can excite those resonances, causing cavity-length fluctuations that, in turn, result in wavelength and power fluctuations. The latter are illustrated in the inset of Fig. 7, where the laser signal is detected by a fast photodiode, followed by an electrical spectrum analyzer (ESA). The fundamental resonance measured at 288 kHz matches closely that obtained from the LDV experiment, implying that the resonance frequencies can be determined likewise from mechanical or optical measurements.

The ESA spectra in Fig. 8 show the resonance peaks of VCSEL-A with $\nu_{res,1} \approx 214$ kHz and $\nu_{res,2} \approx 1250$ kHz ($I_{inj} = 20$ mA). The resolution bandwidth (RBW) for this ESA trace is 100 kHz. Although the amplitude is small (as expected), the plot resembles the behavior shown in Fig. 7. The observed resonance peaks match closely that reported for an electrostatically tunable MEMS-VCSEL in Ref. 23. With the 3 dB bandwidth of $\Delta\nu_{3dB} \approx 70$ kHz of the fundamental resonance as shown in the inset of Fig. 8 (RBW = 1 kHz), we can deduce a quality factor $Q = \nu_{res,1}/\Delta\nu_{3dB} = \omega_0/2\alpha \approx 3$, where $\omega_0 = \sqrt{k_m/m}$ is the ideal (angular) oscillation frequency and $\alpha = R_m/2m$ is the damping factor.[24] This supports the previous assumption of a weakly damped oscillator. With the values of $\nu_{res,1} = 214$ kHz and $m_{eff} = 0.34\,\mu$g, Eq. (5) yields a spring constant $k_m \approx 614.71$ N/m for VCSEL-A. For the MEMS-VCSEL used in the LDV experiment (VCSEL-B), Eq. (5) yields a spring constant $k_m \approx 1075$ N/m. The difference between the two measurements may be due to the

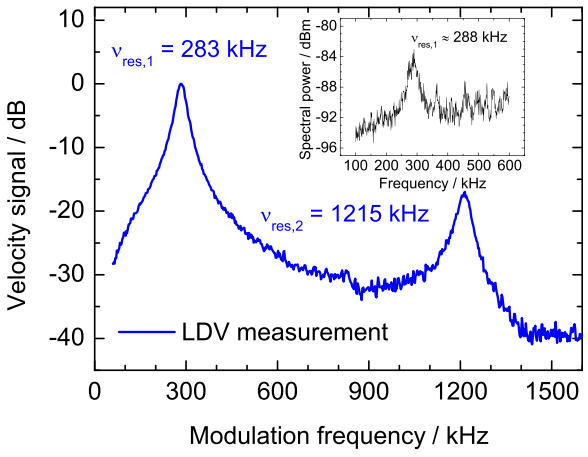

FIG. 7. LDV measurement showing the resonance peaks of VCSEL-B under no-lasing operation. Inset: ESA spectra displaying the fundamental resonance under lasing operation.

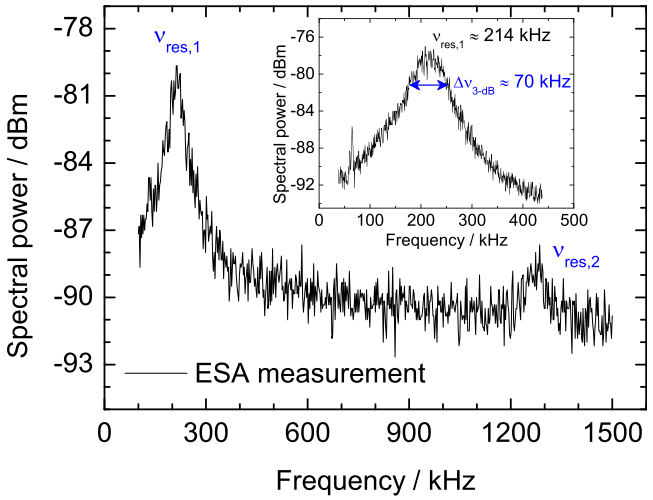

FIG. 8. ESA spectra showing the resonance peaks of VCSEL-A under lasing operation with $I_{inj} = 20$ mA. The inset shows a zoom of the fundamental resonance with a 3 dB bandwidth of 70 kHz.

different characteristic of VCSELs from two different wafers and processing runs.

The spring constant and mechanical resonances have direct consequences for the laser linewidth and stability. Thermal noise induced by Brownian motion results in an average membrane fluctuation.[20,21] Any system at thermal equilibrium with nonzero temperature T has an average energy of $\frac{1}{2}k_BT$ in each degree of freedom, where k_B is Boltzmann's constant. The associated potential energy of the membrane is $E_{pot} = \frac{1}{2}k_m x^2$. The mean-square displacement of the membrane can be written as

$$\frac{1}{2}k_m\langle\Delta x^2\rangle = \frac{a}{2}k_BT, \tag{6}$$

where a represents the degrees of freedom of the system. In the following, we assume that the system is governed mainly by the fundamental oscillation, with little influence of higher-order modes, which is supported by the measurements shown in Fig. 7; hence, $a \approx 1$. If the membrane is displaced by an amount Δx with respect to its equilibrium position, the corresponding change in lasing frequency $\Delta\nu$ is given by[20]

$$\Delta\nu = \frac{2\nu\,\Delta x \cdot \mathrm{FSR}_\nu}{c} \approx \frac{2c\,\Delta x \cdot \mathrm{FSR}_\lambda}{\lambda^3}, \tag{7}$$

where FSR_ν and FSR_λ are the FSRs in the frequency and wavelength domains, respectively. Inserting Eq. (6) in Eq. (7) yields the root-mean-square (rms) fluctuations of the MEMS-VCSELs

$$\Delta\nu_{rms} = \sqrt{\langle\Delta\nu^2\rangle} = \frac{2c \cdot \mathrm{FSR}_\lambda}{\lambda^3}\sqrt{\frac{ak_BT}{k_m}}. \tag{8}$$

For VCSEL-A with $k_m = 614.71$ N/m, $T = 295$ K, $\mathrm{FSR}_\lambda = 92$ nm, and $\lambda = 1550$ nm, Eq. (8) predicts a bandwidth of $\Delta\nu_{rms} = 38.15$ MHz for the inevitable Brownian-motion-induced fluctuations. For VCSEL-B with $k_m \approx 1075$ N/m, $T = 295$ K, $\mathrm{FSR}_\lambda = 82$ nm, and $\lambda = 1560$ nm, Eq. (8) yields a bandwidth of 25.21 MHz.

To measure the linewidth, we employ the delayed self-heterodyne (DSH) technique, which uses a decorrelation-fiber length of 5 km, providing a time delay $\tau_d = 25\,\mu$s. This sufficiently long fiber allows us to measure linewidth and the influence of noise at a frequency above $\nu_d = 1/\tau_d = 40$ kHz.[6,25] In particular, this also includes the mechanical fluctuations of the membrane at ≈ 280 kHz, but excludes slow (thermal) drifts. In principle, the intrinsic linewidth of a laser is of Lorentzian shape. However, inherent Brownian motion and external noise perturbing the membrane, spurious noise pick-ups by the contact needles of the membrane, and changes in the laboratory environment are of statistical nature, with Gaussian spectra. Therefore, an ESA displaying the DSH signal $\Delta\nu_{DSH}$ has weighted contributions from both Gaussian and Lorentzian profiles and is fitted by a Voigt profile, from which the linewidth $\Delta\nu$ is calculated according to Ref. 16, $\Delta\nu = \Delta\nu_{DSH}/\sqrt{2}$. Figure 9 shows the corresponding linewidth of VCSEL-B as a function of the inverse optical power ($T_s = 22\,^\circ$C, $I_{MEMS} = 0$ mA). The linewidth increases almost linearly with the inverse optical power.[26] At the highest power levels, however, the linewidth increases again, possibly owing to the increased heating of the laser cavity. The slope of the linear fit to the experimental data gives an average linewidth– power product of $\Delta\nu \cdot P \approx (1.62 \pm 0.04\,\mathrm{MHz}) \cdot \mathrm{mW}$. Before linewidth broadening, the lowest value of ≈ 41.2 MHz with $I_{inj} = 20$ mA is obtained around an emission wavelength of 1560 nm. The intrinsic linewidth with this injection current is estimated from the Lorentzian part of the Voigt fit as $\approx 12 \pm 4$ MHz, which is very close to the linewidth of a 1550 nm commercial nontunable VCSEL with fixed dielectric mirrors from the manufacturer of the half-VCSEL (VERTILAS). The geometric average of this value and the already-calculated Brownian-fluctuation bandwidth of ≈ 25.21 MHz is $\approx 27.92 \pm 1.5$ MHz. This is in good agreement with the linewidth of $\approx 32.72 \pm 0.95$ MHz obtained from the y-axis intercept ($P = \infty$) of the linear fit. Similarly, for VCSEL-A, a total linewidth of $\approx 39.99 \pm 1.20$ MHz is obtained from the geometric average of the intrinsic linewidth and the Brownian-fluctuation bandwidth of 38.15 MHz.

It is of particular importance for THz photomixing that the laser linewidth does not change considerably over the entire tuning range of a longitudinal mode and that no mode

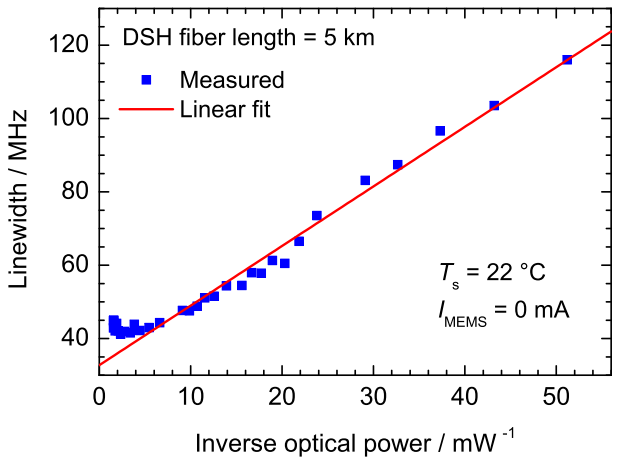

FIG. 9. MEMS-VCSEL (VCSEL-B) linewidth as a function of the inverse optical power ($I_{MEMS} = 0$ mA).

hop occurs within the tuning range of interest. Therefore, the substrate temperature of VCSEL-B is changed from 22 °C to 28 °C. The increase in substrate temperature results in a large blueshift of the emission wavelength for MEMS-VCSEL.[16,27] The reason is that the thermal expansion of the half-VCSEL materials is greater than that of the membrane dielectrics. The consequent greater lateral expansion of the half-VCSEL pulls down the suspended mirror, decreasing the air gap, i.e., blueshifting the emission wavelength. Figure 10 shows the linewidth and corresponding emission wavelength as functions of the membrane current ($I_{inj} = 20$ mA). At both ends, the sharp rise in the linewidth indicates a longitudinal mode hop. The lowest value of ≈ 48 MHz at ≈1560 nm is obtained with $I_{MEMS} = 36$ mA. The difference between this value and the value of 41.2 MHz ($I_{inj} = 20$ mA, $\lambda \approx 1560$ nm) in Fig. 9 can be attributed to the additional Gaussian noise coming from the increased substrate temperature, additional LDC membrane biasing, and radio-frequency pickups by the exposed contact needles of the membrane. However, for the desired wavelength range covered by an EDFA from 1530 to 1565 nm, the linewidth remains below 50 MHz.

It is worth mentioning that the DSH technique employed here records the linewidth on the time scale of 25 μs (40 kHz) generated by the 5 km fiber-optic delay. Therefore, slower drifts cannot be recorded, because the two heterodyned signals remain correlated within the respective time scales. To prevent long-term drifts of the MEMS-VCSELs, a wavelength-locking circuit has been developed employing electrothermal feedback.[7] The electrothermal frequency response shown in Fig. 6 permits the suppression of noise sources with frequencies below ≈ 259 Hz. However, noise sources with frequencies above ≈ 259 Hz cannot be compensated by the developed circuit. We therefore expect the MEMS-VCSELs to fluctuate around the locking point. To determine the low-frequency stability, VCSEL-A is wavelength-locked and subjected to optical beats from a DFB diode that has a linewidth of 2 MHz and a long-term stability of the same order. The corresponding ESA trace in Fig. 11 shows the instantaneous, i.e., short-time-scale, heterodyned linewidth with a single sweep time of 50 ms. Several frequency jumps can be observed originating from the

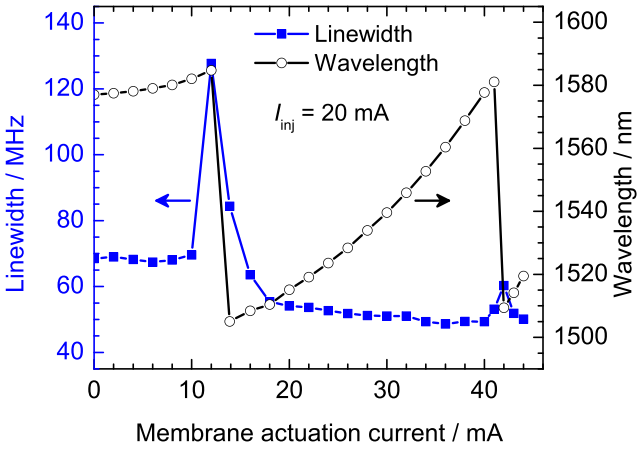

FIG. 10. Linewidth over the tuning range as a function of the membrane actuation current ($I_{inj} = 20$ mA).

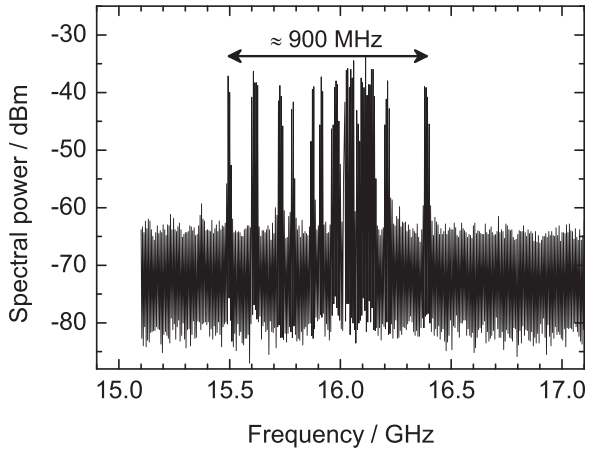

FIG. 11. Wavelength/frequency fluctuations of the heterodyned beat signal of the DFB diode and wavelength-locked MEMS-VCSEL (VCSEL-A).

frequency drifts of VCSEL-A. These drifts are due to several noise sources, such as spurious noise pickups by the contact needles connected to the membrane and acoustic excitation of the membrane itself, as well as to temperature drifts. To examine the associated long-term linewidth, the signal shown in Fig. 11 is time-integrated for 20 s. The corresponding ESA trace in Fig. 12 (RBW = 1 MHz) displays the long-term stability of the heterodyned linewidth with a fluctuation bandwidth $\Delta\nu = 331$ MHz. Since the DFB diode features a long-term linewidth of only $\Delta\nu_{DFB} \approx 2$ MHz, the fluctuation bandwidth of 331 MHz arises solely from the drifts of VCSEL-A. Although this is about an order of magnitude larger than the linewidth of the VCSEL, it is still sufficient for THz spectroscopy at ambient pressure and temperature. Employing electrostatic stabilization for the electrostatically tunable MEMS-VCSELs would allow coverage of the mechanical bandwidth of the fluctuations of ≈ 280 kHz. In this case, MEMS-VCSELs could be conveniently stabilized toward a linewidth of a few tens of MHz.

D. Polarization stability

The photomixing process requires two lasers of the same polarization. Therefore, photomixing setups are usually

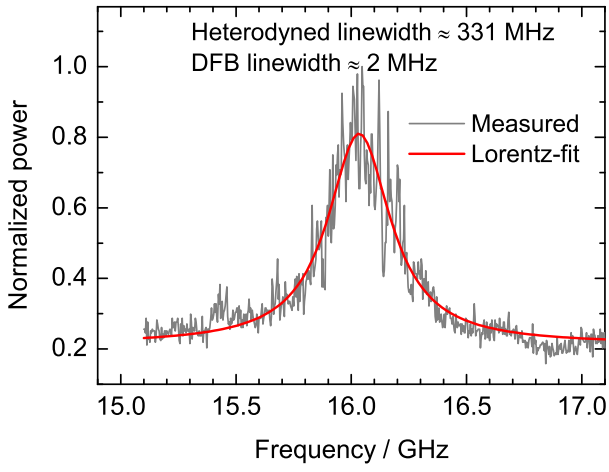

FIG. 12. Lorentzian fit to the time-averaged beat signal, showing an effective fluctuation bandwidth of 331 MHz.

constructed using polarization-maintaining (PM) fibers. On the one hand, polarization stability for MEMS-VCSELs is achieved by incorporating a certain degree of anisotropic gain/loss in the MQWs to break the polarization degeneracy.[28] The incorporated anisotropy avoids polarization switching between the low-indexed crystal directions of the active medium. On the other hand, the membrane itself can act as a polarization-selective reflector incorporating anisotropic losses. This applies particularly to a membrane with geometrical asymmetries, i.e., with different radii of curvature in the respective transverse directions resulting from processing inaccuracies or stress in the membrane.

To characterize the polarization behavior of the MEMS-VCSEL (VCSEL-A), the emitted beam is measured by a large-area photodiode (PD) after passing through a rotatable polarizer. The power emitted along the main emission axis of VCSEL-A is denoted by P_{par}, and that emitted in the direction orthogonal to the first one by P_{orth}. Figure 13 shows both of these as functions of the injection current with $I_{MEMS} = 23.86$ mA and $T_s = 22\,^{\circ}$C. VCSEL-A is polarization-stable, with a parallel-to-orthogonal polarization suppression ratio (PSR) > 20 dB for injection currents in the range 8.75–26 mA. The maximum PSR of ≈ 23 dB is obtained with $I_{inj} = 25$ mA (≈ 1550 nm), but is limited by the polarization–extinction ratio of the setup. Figure 14 shows the polarization-resolved CW tuning of the MEMS-VCSEL with $I_{inj} = 20$ mA. Excellent stability, with PSR >20 dB, is maintained for membrane currents in the range 0–26.5 mA (1525–1556 nm), while the maximum PSR of >24 dB is obtained at $I_{MEMS} = 9.6$ mA. The PSR decreases at higher membrane currents, with the minimum value of ≈ 12 dB being obtained for $I_{MEMS} = 37.58$ mA. Tilt of the suspended membrane caused by fabrication inaccuracies could result in degradation of the polarization, for instance, if the beams holding the membrane are slightly different. Depending on the nature of the initial asymmetry, any significant mechanical movement of the membrane could cause a substantial tilt, which in turn could favor the opposite polarization. Both electrothermal heating and substrate temperature affect the tilt and internal stress of the mirror membrane. For VCSEL-A, a value of $d\lambda/dT_s \approx -9.5$ nm/K

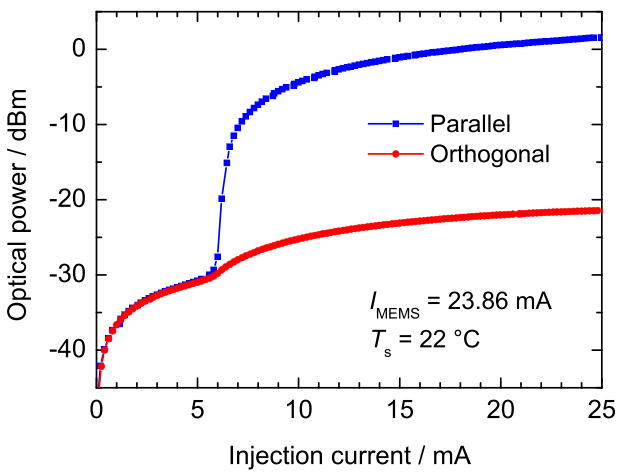

FIG. 13. Polarization-resolved *L-I* characteristics of VCSEL-A with $I_{MEMS} = 23.86$ mA, $\lambda \approx 1550$ nm, $T_s = 22\,^{\circ}$C.

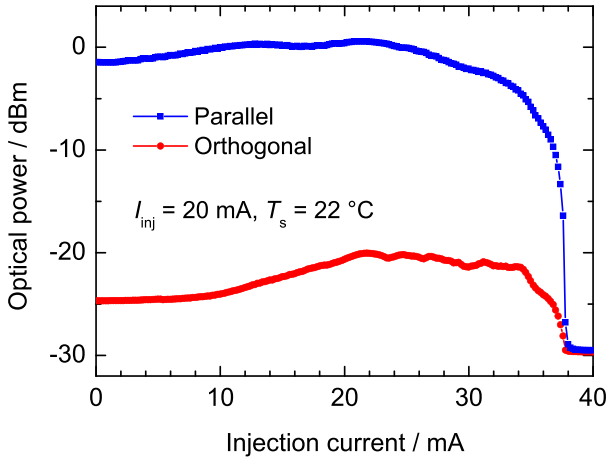

FIG. 14. Polarization-resolved CW tuning for $T_s = 22\,^{\circ}$C.

causes a downward mechanical movement of the membrane of $\approx 2.54\,\mu$m (Ref. 27) for a temperature rise from 22 °C to 50 °C.[27] For $I_{inj} = 20$ mA and $T_s = 50\,^{\circ}$C, P_{par} and P_{orth} are shown in Fig. 15 as functions of the membrane current. With increasing membrane current, the polarization switches at $I_{MEMS} \approx 36$ mA. With decreasing membrane current, it switches at $I_{MEMS} \approx 28.6$ mA, giving rise to hysteresis-like behavior.

E. VCSEL-based THz photomixing setup

Figure 16 shows the experimental setup for THz photomixing. A DFB diode and the MEMS-VCSEL (VCSEL-A) drive a pair of commercial photomixers from TOPTICA Photonics/Fraunhofer-Institut für Nachrichtentechnik. The injection current and stabilized substrate temperature are 20 mA and 22° C, respectively. The emission wavelength is 1525 nm with $I_{MEMS} = 0$ mA, as shown in Fig. 3. The optical power is coupled to a PM fiber through an aspheric lens, aligned to the slow axis of the PM fiber. The coupled power in the fiber is 1.5 mW, 1% of which is tapped out for the wavelength-locking and sweep circuit.[7] The remaining power is directed to the 95% port of a 95/5 PM coupler, where the

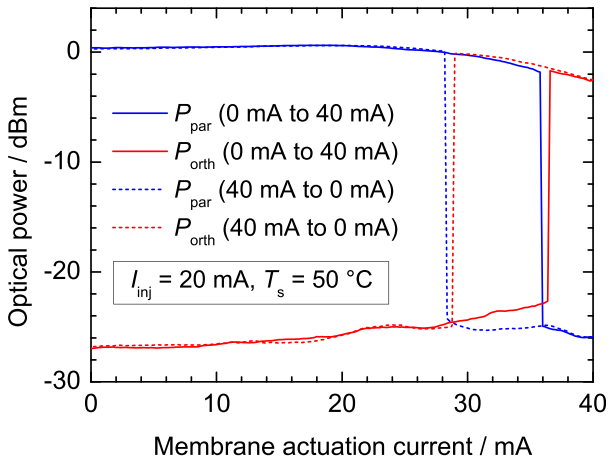

FIG. 15. Polarization switch of VCSEL-A as a function of increasing (0 to 40 mA) and decreasing (40 to 0 mA) membrane current with $I_{inj} = 20$ mA and $T_s = 50\,^{\circ}$C.

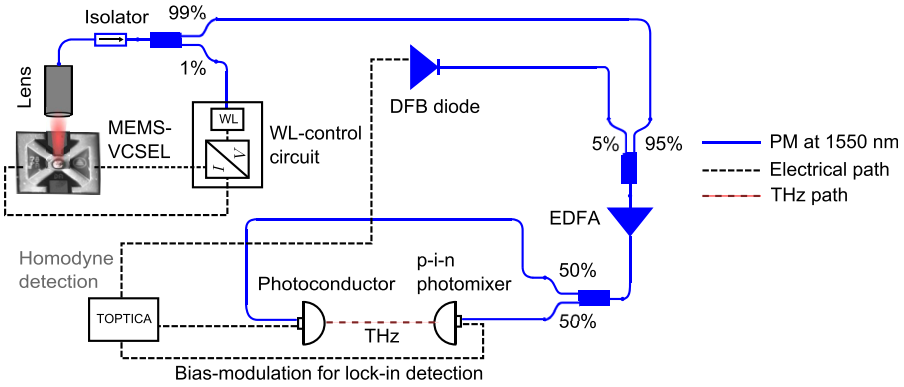

FIG. 16. Schematic of the experimental THz setup, with broadband tunability being accomplished by employing the polarization-stable tunable MEMS-VCSEL (VCSEL-A) at telecommunication wavelengths.

DFB laser feeds the 5% port with a power of about 40 mW. An unequal coupling from the two lasers balances the power levels at the output port. A gain-flattened PM-EDFA (PriTel, Model PMFA-20-IO) amplifies the combined power to ≈ 44 mW. The polarization-matched, equal-amplitude power from the two lasers features a (tunable) difference frequency in the THz range, which drives a p–i–n photomixer (WIN-PD from Fraunhofer-Institut für Nachrichtentechnik/TOPTICA Photonics). An antenna radiates the THz emission in free space. The THz detection is accomplished by employing a photoconductor for homodyne detection using a lock-in amplifier with a time constant τ_{LIA} of 30 or 300 ms. The THz frequency bandwidth of this setup is 2.75 THz, limited by the dynamic range of the detector–source pair at the given laser power. In comparison with the previously reported non-PM setup[7] with a separate amplifier for each laser source, this setup is drastically simplified, using only one amplifier and only PM components at 1550 nm.

To demonstrate the continuous tunability and frequency coverage of the homodyne THz setup, VCSEL-A is tuned and stabilized by the control circuit to a particular wavelength between 1533.41 and 1570.41 nm covering the whole amplification range of the EDFA. First, VCSEL-A is locked to 1533.41 nm. Optical beating of VCSEL-A with the longest DFB laser wavelength of 1558.57 nm generates a bandwidth of 3.14 THz. A subsequent temperature tuning of the DFB laser in steps of 100 MHz is carried out over its tuning range of ≈ 550 GHz, i.e., from 1558.57 to 1554.16 nm. Subsequently, the control circuit tunes and locks VCSEL-A to a longer wavelength with a step of 3–4 nm (corresponding to either ≈ 400 or ≈ 500 GHz steps) followed by repeated temperature tuning of the DFB laser. The wavelength step size of the VCSEL ensures overlap of the individual DFB sweeps to get a continuous spectrum without any interruption. A scan with $\lambda_{VCSEL\text{-}A} < \lambda_{DFB}$ is shown in Fig. 17, where the individual DFB sweeps are indicated by color sequences. The swept THz bandwidth from 3.14 THz to dc is limited solely by the noise floor of the photomixing system to 2.75 THz. Since the setup is operated in ambient air, several water lines are clearly visible. To ensure rapid data acquisition, most data are recorded with $\tau_{LIA} = 30$ ms. Only for the three traces above 1.95 THz (the green, black, and green traces in Fig. 17) is $\tau_{LIA} = 300$ ms used to reduce the noise floor and extend the THz bandwidth. For $\tau_{LIA} = 300$ ms, a dynamic range of ≈ 87.5 dB is obtained at 0.1 THz, while this drops to ≈ 50.3 dB at 1 THz. For $\tau_{LIA} = 30$ ms, the dynamic range is 10 dB smaller, as also shown in Fig. 17. In a similar way, Fig. 18 shows a scan from dc to 1.99 THz for $\lambda_{VCSEL\text{-}A} > \lambda_{DFB}$. In this case, the THz bandwidth is limited by the bandwidth of the PM-EDFA to a maximum difference frequency of 1.99 THz. Therefore, the measurement demonstrates a fully covered bandwidth of 4.74 THz (2.75 THz + 1.99 THz). This is 1.51 THz larger than the result previously reported by our group.[7] Improved photomixers with an extended bandwidth

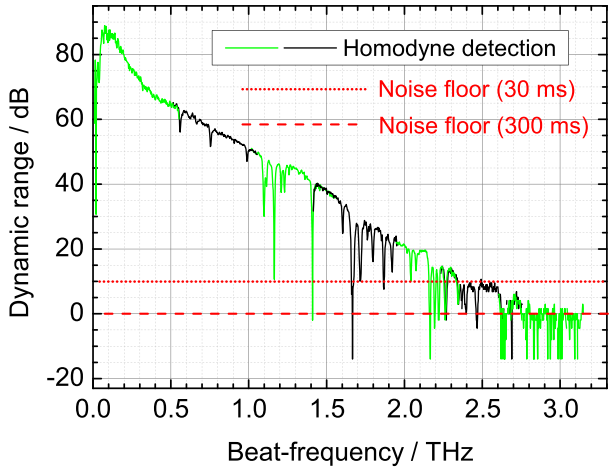

FIG. 17. Homodyne detection up to 2.75 THz for $\lambda_{VCSEL\text{-}A} < \lambda_{DFB}$. The individual DFB sweeps are indicated by color sequences. Several water lines are clearly visible.

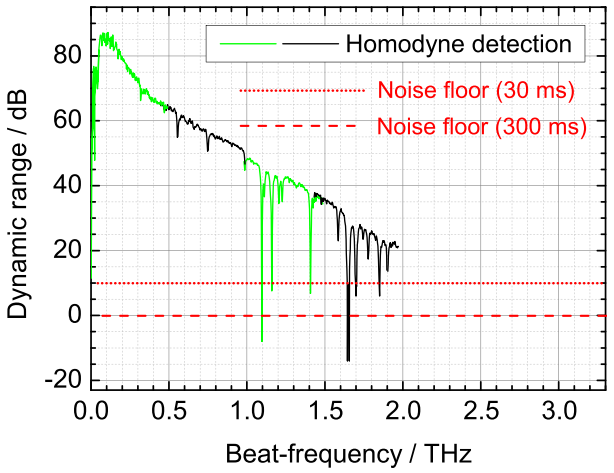

FIG. 18. Homodyne detection up to 1.99 THz for $\lambda_{VCSEL\text{-}A} > \lambda_{DFB}$.

should allow for a sweep up to a THz bandwidth of 4.74 THz using the present optical system with an appropriately chosen DFB diode featuring a wavelength at the edge of the EDFA gain region.

III. CONCLUSION AND OUTLOOK

The performance of a polarization-stable, electrothermally tunable MEMS-VCSEL has been investigated in detail with the aim of using it in a tunable THz photomixing system with an unprecedented bandwidth. Mode-hop-free THz sweeping with an SMSR >50 dB covers a total span of 4.74 THz. The THz bandwidth is limited solely by the dynamic range of the setup and the bandwidth of the EDFA that is used, not by the MEMS-VCSEL, which offers an electrothermal tuning of 64 nm, corresponding to a maximum bandwidth of 7.92 THz. The MEMS-VCSEL is polarization-stable, provides a maximum fiber-coupled power of 1.5 mW, and features a linewidth below 50 MHz over the entire tuning range. It is therefore well suited for THz photomixing systems. As far as wavelength stability is concerned, noise from electronic, acoustic, and mechanical sources causes long-term frequency fluctuations of the on-wafer MEMS-VCSEL of 331 MHz over a time span of 20 s. Packaging and isolation from acoustic and electronic noise sources should improve stability. Further fluctuations can be canceled using a fast wavelength-locking circuit employing electrostatic stabilization with a locking bandwidth significantly above the mechanical resonance frequencies of the membrane DBR ($\approx$ 280 kHz for the first-order resonance and $\approx$1.2 MHz for the third-order resonance), stabilizing toward the intrinsic linewidth of about 40 MHz. Such electrostatically tunable MEMS-VCSELs will be the subject of future work.

ACKNOWLEDGMENTS

This work was supported by the Hessian LOEWE–Sensors Towards Terahertz program and the German Federal Ministry of Education and Research (BMBF) under the VCSEL-TRX project (Grant No. 13N12519). The authors are grateful to Christian Gierl for his significant contribution to the development of the surface micromachining process for the DBR membrane.[7]

[1]K. Iga, "Surface-emitting laser-its birth and generation of new optoelectronics field," IEEE J. Sel. Top. Quantum Electron. **6**, 1201–1215 (2000).
[2]K. Iga, "Vertical-cavity surface-emitting laser (VCSEL)," Proc. IEEE **101**, 2229–2233 (2013).
[3]C. Gierl, T. Gründl, P. Debernardi, K. Zogal, C. Grasse, H. A. Davani, G. Böhm, S. Jatta, F. Küppers, P. Meißner, and M.-C. Amann, "Surface micromachined tunable 1.55 μm-VCSEL with 102 nm continuous single-mode tuning," Opt. Express **19**, 17336–17343 (2011).
[4]S. Paul, C. Gierl, J. Cesar, Q. T. Le, M. Malekizandi, B. Kögel, C. Neumeyr, M. Ortsiefer, and F. Küppers, "10-gb/s direct modulation of widely tunable 1550-nm MEMS VCSEL," IEEE J. Sel. Top. Quantum Electron. **21**, 436–443 (2015).
[5]B. Kögel, K. Zogal, S. Jatta, C. Grasse, M.-C. Amann, G. Cole, M. Lackner, M. Schwarzott, F. Winter, and P. Meissner, "Micromachined tunable vertical-cavity surface-emitting lasers with narrow linewidth for near infrared gas detection," Proc. SPIE **7266**, 72660O–72660O-6 (2008).
[6]D. D. John, C. B. Burgner, B. Potsaid, M. E. Robertson, B. K. Lee, W. J. Choi, A. E. Cable, J. G. Fujimoto, and V. Jayaraman, "Wideband electrically pumped 1050-nm MEMS-tunable VCSEL for ophthalmic imaging," J. Lightwave Technol. **33**, 3461–3468 (2015).
[7]M. T. Haidar, S. Preu, S. Paul, C. Gierl, J. Cesar, A. Emsia, and F. Küppers, "Widely tunable telecom MEMS-VCSEL for terahertz photomixing," Opt. Lett. **40**, 4428–4431 (2015).
[8]M. Tonouchi, "Cutting-edge terahertz technology," Nat. Photonics **1**, 97–105 (2007).
[9]S. Koenig, D. Lopez-Diaz, J. Antes, F. Boes, R. Henneberger, A. Leuther, A. Tessmann, R. Schmogrow, D. Hillerkuss, R. Palmer, T. Zwick, C. Koos, W. Freude, O. Ambacher, J. Leuthold, and I. Kallfass, "Wireless sub-THz communication system with high data rate," Nat. Photonics **7**, 977–981 (2013).
[10]S. Preu, G. H. Döhler, S. Malzer, L. J. Wang, and A. C. Gossard, "Tunable, continuous-wave terahertz photomixer sources and applications," J. Appl. Phys. **109**, 061301 (2011).
[11]H. Ito, F. Nakajima, T. Furuta, and T. Ishibashi, "Continuous THz-wave generation using antenna-integrated uni-travelling-carrier photodiodes," Semicond. Sci. Technol. **20**, S191–S198 (2005).
[12]A. J. Deninger, A. Roggenbuck, S. Schindler, and S. Preu, "2.75 THz tuning with a triple-DFB laser system at 1550 nm and InGaAs photomixers," J. Infrared, Millimeter, Terahertz Waves **36**, 269–277 (2014).
[13]M. Larson, A. Bhardwaj, W. Xiong, Y. Feng, X. d. Huang, K. Petrov, M. Moewe, H. Ji, A. Semakov, C. Lv, S. Kutty, A. Patwardhan, N. Liu, Z. Li, Y. Bao, Z. Shen, S. Bajwa, F. Zhou, and P. C. Koh, "Narrow linewidth sampled-grating distributed bragg reflector laser with enhanced side-mode suppression," in *Optical Fiber Communication Conference* (The Optical Society, 2015).
[14]Y. Matsui, D. Mahgerefteh, X. Zheng, X. Ye, K. McCallion, H. Xu, M. Deutsch, R. Lewén, J. O. Wesström, R. Schatz, and P. J. Rigole, "Widely tuneable modulated grating y-branch chirp managed laser," in *2009 35th European Conference on Optical Communication* (2009), Vol. 2009, pp. 1–2.
[15]M. Müller, W. Hofmann, T. Gründl, M. Horn, P. Wolf, R. D. Nagel, E. Rönneberg, G. Böhm, D. Bimberg, and M.-C. Amann, "1550-nm high-speed short-cavity VCSELs," IEEE J. Sel. Top. Quantum Electron. **17**, 1158–1166 (2011).
[16]S. Paul, M. T. Haidar, J. Cesar, M. Malekizandi, B. Kögel, C. Neumeyr, M. Ortsiefer, and F. Küppers, "Far-field, linewidth and thermal characteristics of a high-speed 1550-nm MEMS tunable VCSEL," Opt. Express **24**, 13142–13156 (2016).
[17]A. S. Pine, R. D. Suenram, E. R. Brown, and K. A. McIntosh, "A terahertz photomixing spectrometer: Application to SO_2 self broadening," J. Mol. Spectrosc. **175**, 37–47 (1996).
[18]P. Signoret, F. Marin, S. Viciani, G. Belleville, M. Myara, J. P. Tourrenc, B. Orsal, A. Plais, F. Gaborit, and J. Jacquet, "3.6-mhz linewidth 1.55-μm monomode vertical-cavity surface-emitting laser," IEEE Photonics Technol. Lett. **13**, 269–271 (2001).
[19]A. Caliman, A. Mereuta, G. Suruceanu, V. Iakovlev, A. Sirbu, and E. Kapon, "8 mw fundamental mode output of wafer-fused vcsels emitting in the 1550-nm band," Opt. Express **19**, 16996–17001 (2011).
[20]R. S. Tucker, D. M. Baney, W. V. Sorin, and C. A. Flory, "Thermal noise and radiation pressure in MEMS fabry-pérot tunable filters and lasers," IEEE J. Sel. Top. Quantum Electron. **8**, 88–97 (2002).
[21]T. B. Gabrielson, "Mechanical-thermal noise in micromachined acoustic and vibration sensors," IEEE Trans. Electron Devices **40**, 903–909 (1993).
[22]G. M. Rebeiz, *RF MEMS: Theory, Design, and Technology* (John Wiley & Sons, Inc., 2003).
[23]C. Gierl, T. Gründl, P. Debernardi, K. Zogal, H. A. Davani, C. Grasse, G. Böhm, P. Meissner, F. Küppers, and M.-C. Amann, "Surface micromachined MEMS tunable VCSEL at 1550 nm with > 70 nm single mode tuning," Proc. SPIE **8276**, 82760P–82760P-9 (2012).
[24]W. M. Siebert, *Circuits, Signals, and Systems* (MIT PR, 1985).
[25]Y. Rao, W. Yang, C. Chase, M. C. Y. Huang, D. P. Worland, S. Khaleghi, M. R. Chitgarha, M. Ziyadi, A. E. Willner, and C. J. Chang-Hasnain, "Long-wavelength VCSEL using high-contrast grating," IEEE J. Sel.. Top. Quantum Electron. **19**, 1701311–1701311 (2013).
[26]K. Kikuchi, "Effect of 1/f-type FM noise on semiconductor-laser linewidth residual in high-power limit," IEEE J. Quantum Electron. **25**, 684–688 (1989).
[27]C. Gierl, T. Gründl, S. Paul, K. Zogal, M. T. Haidar, P. Meissner, M.-C. Amann, and F. Küppers, "Temperature characteristics of surface micromachined MEMS-VCSEL with large tuning range," Opt. Express **22**, 13063–13072 (2014).
[28]B. Kögel, H. Halbritter, M. Maute, G. Böhm, M.-C. Amann, and P. Meissner, "Singlemode and polarization stable MEMS-VCSEL with broadband tuning characteristics around 1.55 μm," in *2006 European Conference on Optical Communications* (Institute of Electrical and Electronics Engineers, 2006).